RSC Advances

PAPER

View Article Online
View Journal | View Issue



Cite this: *RSC Adv.*, 2025, **15**, 35468

# A comparative study of frustration in Al/P and B/P-based intramolecular frustrated Lewis pairs

Santhosh Guntupalli,† Mohmmad Faizan,† Bhupendra Singh Bisht and Ravinder Pawar *

Received 11th August 2025
Accepted 18th September 2025

DOI: 10.1039/d5ra05892a

rsc.li/rsc-advances

Intramolecular frustrated Lewis pairs (IFLPs) have emerged as versatile systems for small molecule activation, with their reactivity critically influenced by the nature of the bridging unit and the intrinsic properties of the Lewis acid and base. In this work, we present a comparative computational analysis of AlP- and BP-based IFLPs featuring a series of structurally analogous linkers. Using $H_2$ activation as a unified metric, we evaluate the degree of frustration encoded within each system by examining transition state energetics, adduct stability, and electronic structure features. Our findings reveal that while AlP-IFLPs often exhibit masked behavior due to partial Al–P interactions, their BP counterparts remain classical FLPs with greater spatial separation. The geminal-bridged $AlP_{Gem}$ system exhibits the most favorable energetic profile, whereas rigid systems like $AlP_{Nap}$ incur substantial strain. This study underscores the role of both electronic and geometric parameters in dictating FLP behavior and provides valuable insights for the rational design of future IFLPs with enhanced reactivity and tunability.

## Introduction

Since the pioneering work by Stephan and co-workers in 2006 on the metal-free activation of dihydrogen using sterically encumbered Lewis acid–base pairs, the concept of Frustrated Lewis Pairs (FLPs) has emerged as a powerful platform for small molecule activation and catalysis.[1] In conventional Lewis acid–base adducts, the acid and base form a stable dative bond. However, in FLPs, such bonding is hindered by steric or geometric constraints, resulting in reactive acid–base pairs that can activate otherwise inert substrates.[2–13] FLPs are generally classified into three types: intermolecular, intramolecular, and masked (or hidden) FLPs.[14] Intermolecular FLPs involve separate Lewis acid and base moieties, typically with bulky substituents to prevent adduct formation. In contrast, intramolecular FLPs (IFLPs) tether both the acid and base within a single molecule *via* a linker, offering improved control over the proximity and orientation of the reactive sites. Masked FLPs appear as classical Lewis adducts in the solid state but dissociate in solution or under strain, exhibiting FLP-like reactivity under specific conditions.[14]

Since their discovery, FLPs have demonstrated a wide range of reactivities, particularly in the activation of small molecules such as $H_2$, $CO_2$, $N_2O$, and olefins.[2,15,16] Their applications span metal-free hydrogenation, carbon capture and utilization, C–F and C–H bond activation, and even polymerization catalysis.[17–19] Most commonly, boron-based Lewis acids like $B(C_6F_5)_3$ are employed due to their well-defined synthesis and tunable Lewis acidity. The reactivity of FLPs has been significantly modulated through variations in substituents, the nature of the bridging unit, and by electronic tuning—notably *via* aromatic and anti-aromatic modifications to the acidic or basic sites.[20–28] To expand the chemical space of FLPs and explore new avenues for reactivity, alternative Lewis acid/base combinations have been investigated. In this context, replacing boron with aluminum as the Lewis acidic component presents a particularly appealing strategy.[29] Aluminum, being more acidic than boron, offers the potential for enhanced reactivity, but also presents synthetic and stability challenges.[30] Recent studies have demonstrated that Al-based FLPs can successfully activate a wide range of substrates including $H_2$, $CO_2$, C=O, and C=C bonds.[29,31–33] For example, the intermolecular system $Al(C_6F_5)_3$ combined with bulky phosphines such as $Mes_3P$ or *o*-$Tol_3P$ was found to reversibly activate $H_2$ and $CO_2$, and also engage in olefin hydrogenation and C–F bond activation.[29,33,34] The Al/P FLPs have been shown to catalyze the hydrogenation of ethylene and cyclohexene,[32,34] while another study demonstrated the use of Al FLPs in $CO_2$ reduction to methanol using HBpin as the reductant.[35] Moreover, Uhl and co-workers have reported a geminal Al–P FLP based on a *t*-butyl-substituted aluminum and diphenylphosphine, capable of activating a range of small molecules such as isocyanates, $CO_2$, and organic azides.[36–38]

It is worth noting, however, that despite their higher intrinsic Lewis acidity, Al-based IFLPs have been comparatively less investigated than BP analogues, largely due to experimental

*Laboratory of Advanced Computation and Theory for Materials and Chemistry, Department of Chemistry, National Institute of Technology Warangal (NITW), Warangal, Telangana 506004, India. E-mail: ravinder_pawar@nitw.ac.in*

† The authors have contributed equally.

challenges. The strong oxophilicity and moisture sensitivity of aluminum complicate synthesis and handling, while the preparation of intramolecular Al–P linkages often requires specific synthetic routes such as aluminum–tin exchange. These technical and stability-related difficulties, along with the greater synthetic accessibility of boron precursors, have collectively slowed the broader experimental development of AlP IFLPs. Although various intermolecular Al based FLPs have been extensively studied, examples of intramolecular Al/P FLPs (Al–P IFLPs) remain comparatively limited. A few recent reports have detailed the synthesis and reactivity of Al–P IFLPs with rigid tethers like *ortho*-phenylene or biphenylene, which play a pivotal role in tuning the spatial proximity and interaction of the acid–base sites.[39–41] Such rigid systems can enforce strain that enhances reactivity by favorably preorganizing the reactive centers and lowering activation barriers through enthalpic and entropic contributions. For instance, xanthene- and biphenylene-linked Al–P systems have shown reactivity toward $CO_2$ and other polar substrates, demonstrating that carefully chosen linkers can modulate the degree of frustration and the resulting chemical behavior.[42] Despite these advances, a systematic comparison of Al–P and B–P IFLPs, particularly regarding how the bridging unit affects their reactivity and activation capability, remains lacking. Notably, B–P IFLPs have been more widely investigated across a variety of linkers and substitution patterns, whereas their Al-based counterparts are still in their early stages of exploration. This study aims to fill this gap by providing a comparative analysis of Al–P and B–P intramolecular FLPs, focusing on structurally analogous bridging units that have previously been explored in B–P systems. By studying these systems side by side, we aim to identify trends in reactivity and to understand how the intrinsic Lewis acidity of the central atom (Al *vs.* B) and the choice of linker affect the degree of frustration and bond activation potential.

To this end, a set of representative bridging motifs, commonly used in B/P-FLPs, have been adapted and systematically studied in their Al/P analogues (Fig. 1), enabling direct comparisons and a deeper understanding of structure–activity (*i.e.*, frustration) relationships. The frustration of these FLPs has been evaluated by comparing their calculated $H_2$ splitting energies. Density functional theory (DFT) calculations, along with detailed orbital analyses, have been carried out to gain insight into how the bridging unit, electronic structure, and intrinsic Lewis acidity collectively influence the behavior of these FLP systems.

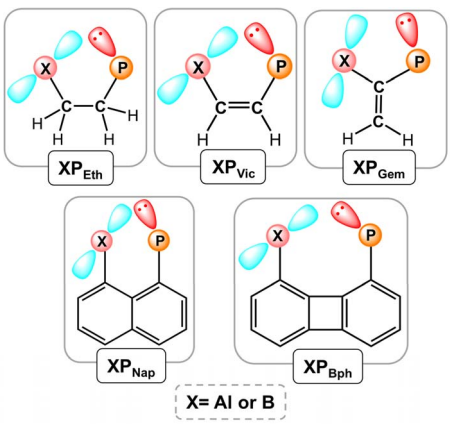


Fig. 1 AlP and BP based IFLPs considered in the present work.

## Computational details

The geometries of the considered IFLPs, transition states (TSs) and adducts (ADs) formed in the reaction of $H_2$ with the considered IFLPs were fully optimized employing M062X functional with 6-311++G** basis set.[43,44] This level of theory was chosen because M06-2X has been extensively benchmarked and shown to provide accurate thermochemistry, kinetics, and noncovalent interaction energies for main-group systems, including frustrated Lewis pairs and $H_2$ activation processes.[45–50] The inclusion of diffuse functions in the 6-311++G** basis set is essential for correctly describing the anionic character that develops at the phosphide site during $H_2$ activation, representing the elongated and polarized H–H bond in transition states, and capturing long-range frustrated interactions between the spatially separated acid–base centers.[45–50] No symmetrical or geometrical constraints were imposed during the optimization. The SMD[51] implicit solvent model was applied using toluene ($\varepsilon = 2.3741$) with the default parameters in Gaussian 16, consistent with previous computational studies on $H_2$ activation by FLPs.[45–50] The harmonic frequency calculations were carried out on the same level of theory to depict the nature of the stationary points as local minima and as first order saddle point. The transition states were confirmed by the presence of single imaginary frequency in the direction of bond alterations. The intrinsic reaction coordinate (IRC) analysis has been carried confirm the TSs as the structures connecting the product with the reactants. The fully optimized structures were then used to study the energetics of the reaction at 1 atm pressure and 298.15 K. The calculations have been performed using Gaussian 16 software.[52] The energetic results were systematically compared. Further to gain insights to the frustration and catalytic behaviour of the IFLPs, NBO have been carried out.[53] The second order perturbation analysis form the NBO is employed to derive the orbital charge transfer analysis. The natural bond orbitals were plotted at 0.02 a.u. iso value. To assess the interaction between the acidic and basic site the quantum theory of atoms in molecule (QTAIM)[54–56] analysis was carried out using Multiwfn software.[57]

To understand the origin of the activation barriers and to dissect the energetic contributions involved in the $H_2$ activation by the investigated IFLPs, the Activation Strain Model (ASM),[58] also referred to as the Distortion–Interaction Model, was employed. In this model, the activation energy ($\Delta E^{\ddagger}$) for the transition state is decomposed into two principal components: strain (or distortion) energy ($\Delta E_{strain}$) and interaction energy ($\Delta E_{int}$). The total activation energy is expressed as:

$$\Delta E^{\ddagger} = \Delta E_{strain} + \Delta E_{int}$$

where, $E_{strain}$ corresponds to the energy required to deform the individual fragments—namely, the FLP and $H_2$—from their optimized geometries in the isolated state to the geometries they adopt in the transition state. The $\Delta E_{int}$ is the stabilizing energy gained from the electronic interaction between the deformed fragments at the transition state geometry. The strain energy for a fragment was calculated as:

$$\Delta E_{strain}\ (\mathrm{FLP}) = E_{FL}^{\mathrm{PTS\text{-}geom}} - E_{FLP}^{opt}$$

$$\Delta E_{strain}\ (H_2) = E_{H_2}^{\mathrm{TS\text{-}geom}} - E_{H_2}^{opt}$$

where $E^{\mathrm{TS\text{-}geom}}$ denotes the single-point energy of the fragment in the geometry it adopts within the transition state, and $E^{opt}$ is the energy of the fully optimized fragment in its equilibrium structure.

The total strain energy is the sum of the individual strain energies:

$$\Delta E_{strain}^{total} = \Delta E_{strain}\ (\mathrm{FLP}) + \Delta E_{strain}\ (H_2)$$

The interaction energy ($\Delta E_{int}$) was then computed as:

$$\Delta E_{int} = E_{TS} - E_{FLP}^{\mathrm{TS\text{-}geom}} - E_{H_2}^{\mathrm{TS\text{-}geom}}$$

where $E_{TS}$ is the total electronic energy of the full transition state complex. This decomposition allows for a quantitative analysis of the balance between geometric distortion and favourable orbital interaction in determining the activation barrier.

## Results

In the present study, the activation energy for $H_2$ splitting has been employed as a uniform metric to assess and compare the degree of frustration across the investigated intramolecular frustrated Lewis pairs (IFLPs). This approach facilitates a consistent comparison of the impact of structural immobilization induced by various bridging units. Accordingly, the relative Gibbs free energies ($\Delta G$) of the transition states (TS-$XP_{Abr}$; X = Al or P, and Abr = Eth, Vic, Gem, Nap, and Bph), along with the free energies of the corresponding adducts formed upon $H_2$ activation, are presented in Fig. 2.

From Fig. 2, it is evident that the $H_2$ activation barrier for the ethyl-bridged AlP system (TS-$AlP_{Eth}$) is 31.4 kcal $mol^{-1}$. This value remains essentially unchanged upon replacing the ethyl bridge with a vinyl group, as seen in TS-$AlP_{Vic}$. The free energy of the adduct in $AlP_{Eth}$ (AD-$AlP_{Eth}$) is calculated to be 24.9 kcal $mol^{-1}$, whereas the corresponding adduct in $AlP_{Vic}$ (AD-$AlP_{Vic}$) has a slightly higher $\Delta G$ of 25.5 kcal $mol^{-1}$, suggesting a marginal destabilization induced by the vinyl bridge.

In contrast, the BP analogue $BP_{Eth}$ exhibits a higher $H_2$ activation barrier of 34.1 kcal $mol^{-1}$, while the $\Delta G$ of its adduct (AD-$BP_{Eth}$) remains comparable to that of AD-$AlP_{Eth}$. Interestingly, upon changing the bridging unit from ethyl to vinyl in the

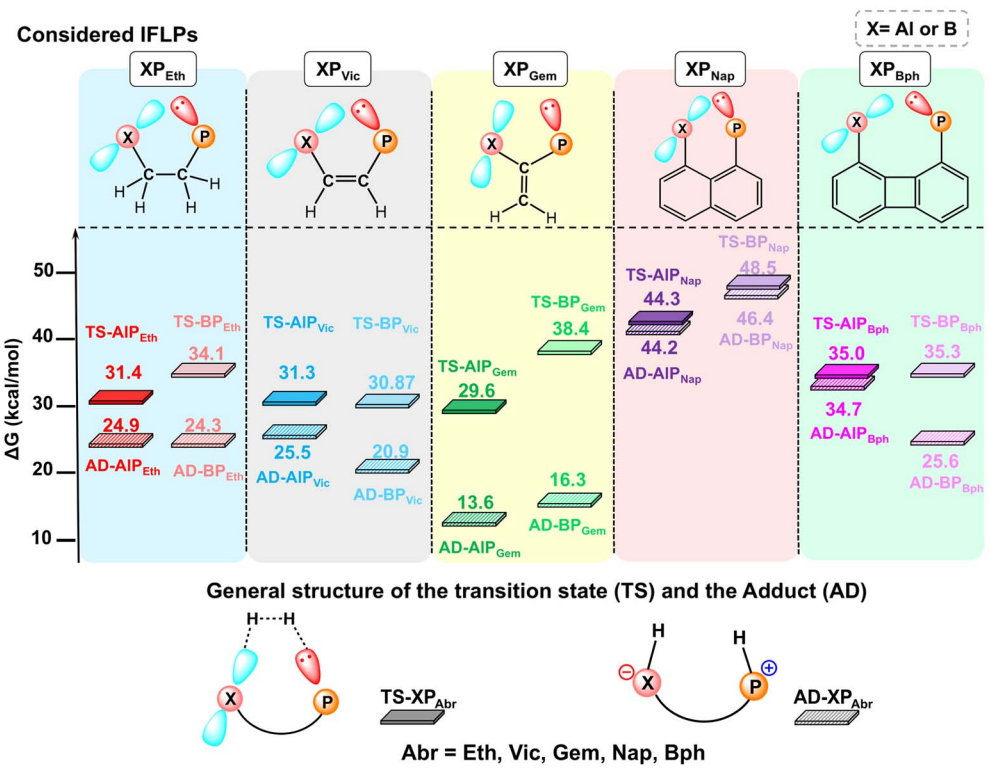


Fig. 2 Relative free energy of the transition state (TS-$XP_{Abr}$, X = Al/B and Abr = Eth, Vic, Gem, Nap, Bph) and the adduct (AD-$XP_{Abr}$) found in the reaction of $H_2$ with considered IFLPs along with their general structures.

BP system, both the transition state (TS-$BP_{Vic}$) and adduct (AD-$BP_{Vic}$) energies decrease by approximately 4 kcal $mol^{-1}$ (see Fig. 2). This trend is notably different from the AlP system, where a similar structural modification yields negligible change. These observations underscore that identical modifications exert distinct effects in AlP-*versus* BP-based IFLPs. Moreover, incorporation of a naphthyl bridging unit leads to the highest $H_2$ activation barriers and adduct $\Delta G$ values among all systems examined. Specifically, both $AlP_{Nap}$ and $BP_{Nap}$ show transition states and adducts with $\Delta G$ values exceeding 44 kcal $mol^{-1}$. In contrast, replacing the naphthyl bridge with a biphenylene unit reduces the activation energy to approximately 35 kcal $mol^{-1}$ in both $AlP_{Bph}$ and $BP_{Bph}$ systems, reflecting a significant energetic improvement. Among all IFLPs studied, the geminal-bridged system $AlP_{Gem}$ exhibits the most favorable energetics, with the lowest $\Delta G$ values for both the transition state (29.6 kcal $mol^{-1}$) and the adduct (13.6 kcal $mol^{-1}$). Conversely, its BP analogue $BP_{Gem}$ shows a much higher transition state energy of 38.4 kcal $mol^{-1}$ which is second only to the naphthyl-bridged cases, while the adduct energy (16.3 kcal $mol^{-1}$) remains relatively low. Overall, these free energy profiles highlight the critical role of structural immobilization in tuning the degree of frustration in IFLPs. Moreover, they clearly demonstrate that AlP- and BP-based IFLPs exhibit distinct energetic trends in response to the same bridging unit modifications. These findings underscore the importance of further investigating the structural and electronic factors governing the reactivity of AlP *versus* BP-based systems.

Accordingly, a detailed analysis of the electronic structures of the studied IFLPs, along with the geometries of their respective transition states and $H_2$-activation adducts, has been undertaken to rationalize these observations. The optimized geometries of $AlP_{Eth}$ and $AlP_{Vic}$, along with their corresponding natural bond orbital (NBO) plots and electron density contour plots, are presented in Fig. 3a and b, respectively. The fully labeled optimized geometries of the transition states (TS) and the respective adducts formed upon reaction with $H_2$ are also depicted in Fig. 3, along with key geometrical parameters. From the geometries shown in Fig. 3a and b, the Al–P bond distances in $AlP_{Eth}$ and $AlP_{Vic}$ are found to be 2.61 Å and 2.58 Å, respectively. Quantum Theory of Atoms in Molecules (QTAIM) analysis

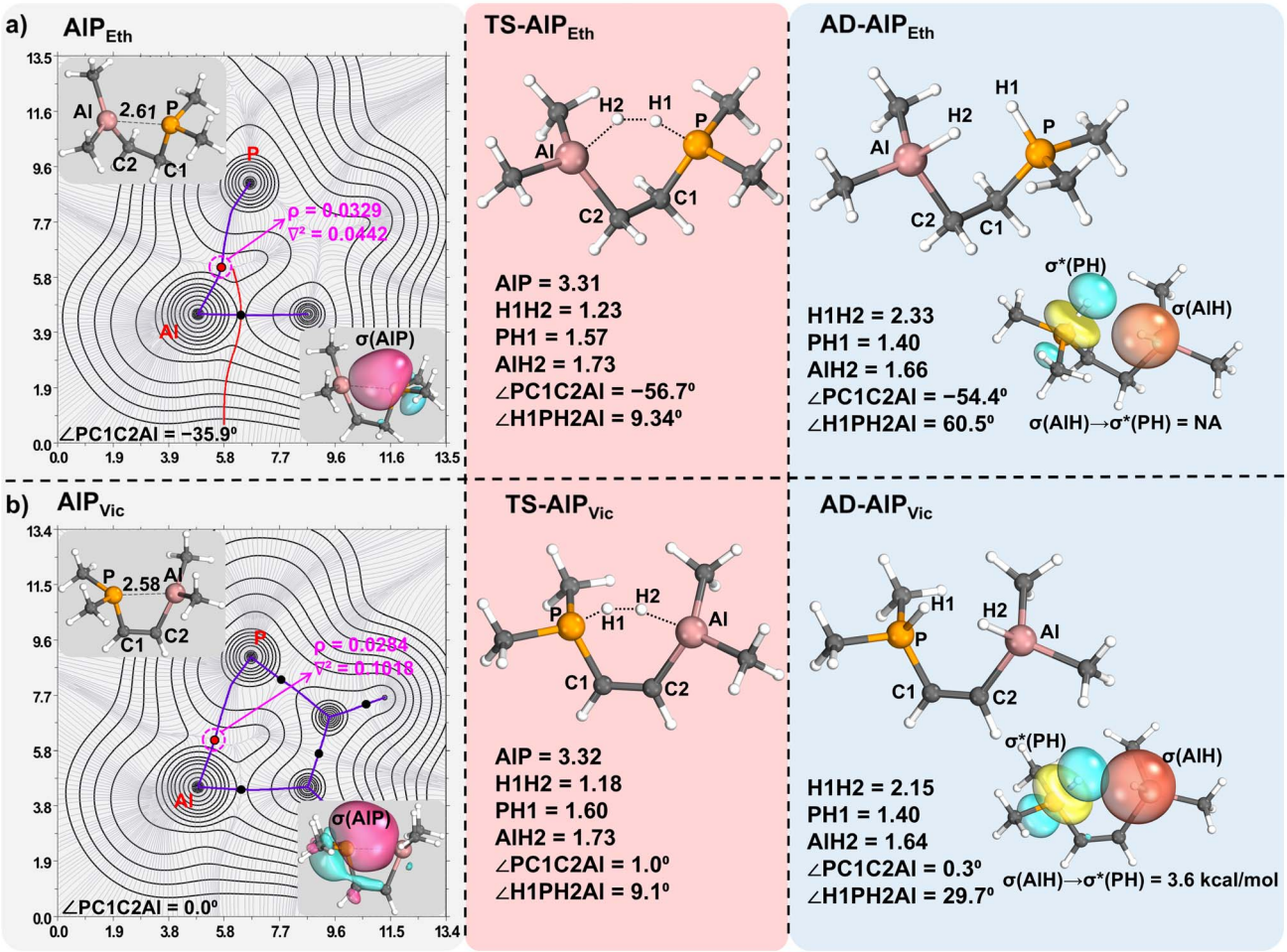


Fig. 3 Optimized geometries of (a) $AlP_{Eth}$ and (b) $AlP_{Vic}$ with electron density contour and natural bond orbital plots along with respective optimized geometries of the transition states and the adducts formed in the reaction of the IFLPs with $H_2$. (All the distances are given in the angstrom, the contours are plotted at 0.001 a.u. iso value and the electron densities at the bond critical points are in a.u.).

reveals the presence of a bond critical point (BCP) between the Al and P atoms in both molecules, with electron density ($\rho$) values of 0.0329 a.u. for $AlP_{Eth}$ and 0.0284 a.u. for $AlP_{Vic}$. The presence of a BCP indicates a significant interaction between the Al and P centres, which is further corroborated by the existence of a σ-bonding orbital between them, as identified in the NBO analysis.

The short Al–P distances, presence of a BCP, and the σ-type bonding interaction collectively suggest that both $AlP_{Eth}$ and $AlP_{Vic}$ exist in the form of masked FLPs. Accordingly, during the reaction with $H_2$, the Al–P bond is expected to elongate to accommodate the incoming dihydrogen molecule. Additionally, analysis of the optimized geometries shows that the dihedral angle ∠P–C1–C2–Al is −35.9° in $AlP_{Eth}$ and 0.0° in $AlP_{Vic}$, suggesting that the C1–C2 bond in $AlP_{Eth}$ allows rotational flexibility, while such rotation is restricted in $AlP_{Vic}$. This distinction becomes more apparent in the transition state structures. In TS-$AlP_{Eth}$, the Al–P distance increases to 3.31 Å, reflecting the elongation required to interact with the $H_2$ molecule. A similar elongation is observed in TS-$AlP_{Vic}$, as shown in Fig. 3b. The H1–H2, P–H1, and Al–H2 bond distances in TS-$AlP_{Eth}$ are 1.23 Å, 1.57 Å, and 1.73 Å, respectively, and the dihedral angle ∠H1–P–Al–H2 is 9.34°, all of which closely match the corresponding values in TS-$AlP_{Vic}$. However, the dihedral angle ∠P–C1–C2–Al changes significantly in TS-$AlP_{Eth}$ it is −56.7°, while in TS-$AlP_{Vic}$ it remains nearly unchanged at 1.0°. This indicates that $AlP_{Eth}$ allows rotational adjustment about the C1–C2 bond during reaction, thereby relieving strain, whereas such flexibility is absent in $AlP_{Vic}$ due to the rigidity of the vinyl bridging unit. The geometric similarities between the two transition states suggest comparable energetic profiles. To investigate this further, strain and interaction energies were calculated. The strain energy developed in $AlP_{Vic}$ upon reaching the transition state was found to be 21.15 kcal $mol^{-1}$, while in $AlP_{Eth}$ it was 18.95 kcal $mol^{-1}$. The slightly higher strain in $AlP_{Vic}$ can be attributed to its restricted rotational freedom, as indicated by the minimal change in the ∠P–C1–C2–Al angle. Conversely, the strain energy within the $H_2$ molecule at the transition state was 38.39 kcal $mol^{-1}$ for TS-$AlP_{Vic}$ and 44.25 kcal $mol^{-1}$ for TS-$AlP_{Eth}$. Consequently, the total strain energy for TS-$AlP_{Vic}$ is 59.54 kcal $mol^{-1}$, slightly lower than 63.20 kcal $mol^{-1}$ for TS-$AlP_{Eth}$. The interaction energies between $H_2$ and the FLPs in their respective transition states were also evaluated. In TS-$AlP_{Vic}$, the interaction energy was −37.33 kcal $mol^{-1}$, which is lower than that of TS-$AlP_{Eth}$ (−40.92 kcal $mol^{-1}$). The reduced interaction energy in $AlP_{Vic}$ may be due to limited access to the reactive site, resulting from the rigid vinyl bridge. This lower interaction energy offsets the lower strain energy in TS-$AlP_{Vic}$, while in TS-$AlP_{Eth}$, the higher strain is compensated by stronger interaction with $H_2$. Overall, these opposing effects result in comparable transition state energies for both systems.

Further, in the adduct structure AD-$AlP_{Eth}$, the H1–H2 distance was found to be 2.23 Å, which is slightly longer than the corresponding distance in AD-$AlP_{Vic}$ (see Fig. 3). The dihedral angles ∠P–C1–C2–Al and ∠H1–P–Al–H2 were calculated to be −54.4° and 60.5°, respectively, in AD-$AlP_{Eth}$, whereas in AD-$AlP_{Vic}$ these values were 0.3° and 29.7°. This difference in dihedral angles further supports the observation that $AlP_{Eth}$ undergoes structural relaxation *via* rotation around the C1–C2 bond, which facilitates a more open geometry. As a result, the newly formed P–H1 and Al–H2 bonds in AD-$AlP_{Eth}$ are spatially oriented away from each other, suggesting minimal interaction between them. In contrast, the restricted rotation in AD-$AlP_{Vic}$ appears to maintain the proximity of these bonds, possibly allowing intramolecular interaction between the hydrogen atoms. This inference is supported by the NBO analysis of AD-$AlP_{Vic}$, which reveals an orbital charge transfer (OCT) from the bonding orbital σ(Al–H2) to the antibonding orbital σ*(P–H1) with an associated stabilization energy of 3.6 kcal $mol^{-1}$ which is absent in the case of AD-$AlP_{Eth}$ (see Fig. 3). This OCT supports the geometric observations made in the adduct structures. Although small, this interaction contributes to weakening of the P–H1 bond in AD-$AlP_{Vic}$, thereby destabilizing the adduct and resulting in a slightly higher $\Delta G$ compared to AD-$AlP_{Eth}$.

Unlike the AlP-based IFLPs, the B–P distances in $BP_{Eth}$ and $BP_{Vic}$ were found to be significantly longer, measuring 3.44 Å and 3.21 Å, respectively (see Fig. S1). Notably, no bond critical point (BCP) or σ-bonding orbital was identified between the B and P atoms in either system, as shown in Fig. S1 in the SI. Instead of a direct σ(B–P) bond, a lone pair orbital at P (lp(P)) and an empty p orbital at B (p(B)) were observed, along with an orbital charge transfer (OCT) from lp(P) to p(B). The corresponding OCT energies were calculated to be 1.59 kcal $mol^{-1}$ for $BP_{Eth}$ and 4.55 kcal $mol^{-1}$ for $BP_{Vic}$. The higher OCT value in $BP_{Vic}$ is likely due to its more rigid structure, which brings the B and P centres closer together, as evidenced by the small dihedral angle ∠P–C1–C2–B of 0.6° in $BP_{Vic}$ compared to the more relaxed geometry in $BP_{Eth}$ (see Fig. S1). These geometrical and electronic features indicate that $BP_{Eth}$ and $BP_{Vic}$ behave as classical, unmasked FLPs, in contrast to the masked nature of the AlP IFLPs. This fundamental difference in bonding and flexibility between B–P and Al–P systems may contribute to their distinct energetic profiles, even under structurally analogous conditions. In the case of the transition state of $BP_{Eth}$ (*i.e.*, TS-$BP_{Eth}$), rather than an increase in B–P distance, as observed for $AlP_{Eth}$, the distance decreases from 3.44 Å in $BP_{Eth}$ to 3.07 Å in TS-$BP_{Eth}$. Additionally, the dihedral angle ∠P–C1–C2–B becomes −51.4°, suggesting a significant structural distortion and strain buildup. The calculated strain energy in TS-$BP_{Eth}$ was 23.71 kcal $mol^{-1}$, which is higher than the corresponding value for TS-$AlP_{Eth}$. Moreover, the interaction energy between $H_2$ and $BP_{Eth}$ in the transition state was calculated to be −36.69 kcal $mol^{-1}$, which is less favourable than that in TS-$AlP_{Eth}$, indicating a higher $\Delta G$ for the reaction pathway in the $BP_{Eth}$ system. In contrast, in going from $BP_{Vic}$ to TS-$BP_{Vic}$ involved only minor changes in structural parameters, resulting in minimal geometric distortion. The overall strain energy in TS-$BP_{Vic}$ was calculated to be 47.70 kcal $mol^{-1}$, which is lower than that observed for TS-$BP_{Eth}$ and contributes to a lower $\Delta G$ for TS-$BP_{Vic}$. Furthermore, as observed in the AlP-based systems, an OCT from σ(B–H2) to the antibonding orbital σ*(P–H1) was absent in AD-$BP_{Eth}$, but present in AD-$BP_{Vic}$, providing an explanation for their relative stabilities (see Fig. S1).

As in the cases of $AlP_{Eth}$ and $AlP_{Vic}$, the electron density contour plots of $AlP_{Nap}$ and $AlP_{Bph}$, shown in Fig. 4, reveal the presence of a bond critical point (BCP) between the aluminum and phosphorus centres. Additionally, natural bond orbital (NBO) analysis confirms the presence of a σ(Al–P) bonding orbital in both systems (see Fig. S2 in the SI). These findings indicate that $AlP_{Nap}$ and $AlP_{Bph}$, like the other AlP-based IFLPs investigated in this study, exhibit the characteristics of masked FLPs. A closer geometrical comparison (Fig. 4) reveals that in $AlP_{Bph}$, the P–C1 and Al–C2 bonds are bent inward toward one another. This geometry arises from intramolecular Al–P interaction, resulting in a strained structure, consistent with previous reports.[39,41] During the formation of the transition state, elongation of the Al–P bond alleviates this strain.

In contrast, the initial structure of $AlP_{Nap}$ is less strained; however, it exhibits the shortest Al–P bond distance *i.e.*, 2.49 Å, among all the AlP IFLPs studied. As a result, when $H_2$ approaches $AlP_{Nap}$ to form the transition state ($TS\text{-}AlP_{Nap}$), significant distortion occurs in the molecule. In the optimized structure of $TS\text{-}AlP_{Nap}$, the Al–P bond length increases to 3.29 Å, and the dihedral angle ∠P–C1–C2–Al changes from 0.0° in the parent molecule to −29.4°. By comparison, in $TS\text{-}AlP_{Bph}$, the Al–P bond length increases to 3.75 Å, and ∠P–C1–C2–Al changes to only −13.5°, suggesting a comparatively lesser degree of distortion. The calculated strain energy in $TS\text{-}AlP_{Nap}$ was found to be 80.87 kcal $mol^{-1}$, which is not only higher than that in $TS\text{-}AlP_{Bph}$ (*i.e.*, 75.12 kcal $mol^{-1}$) but also the highest among all the AlP-based IFLPs studied. This corresponds to the highest Gibbs

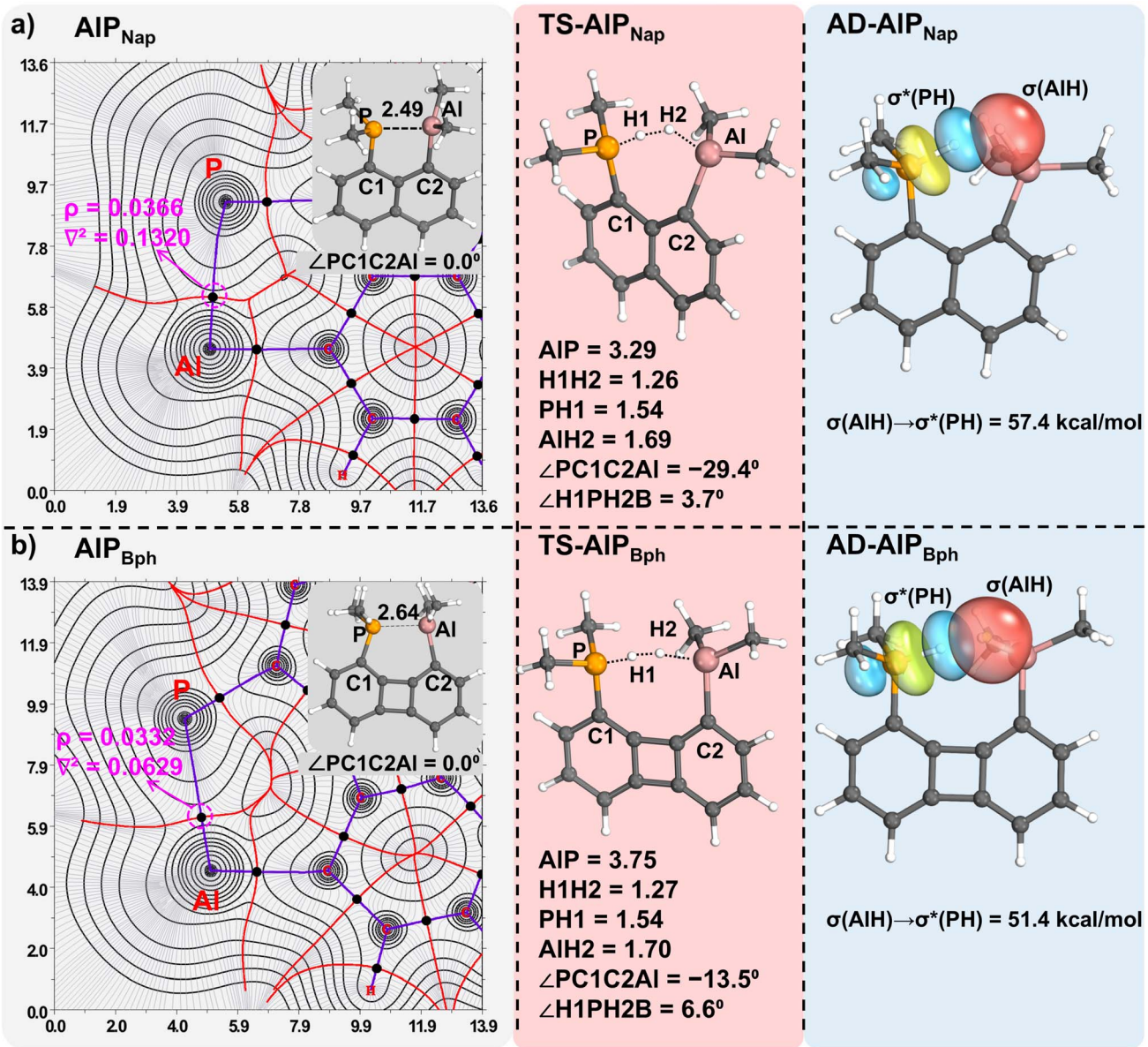


Fig. 4 Electron density contour plots and optimized geometries of (a) $AlP_{Nap}$ and (b) $AlP_{Bph}$, along with their corresponding transition state structures and natural bond orbital (NBO) plots, highlighting key orbital charge transfer (OCT) interactions observed in the adducts. (All the distances are given in the angstrom, the contours are plotted at 0.001 a.u. iso value and the electron densities at the bond critical points are in a.u.).

free energy ($\Delta G$) for $H_2$ activation in this series, underscoring the energetic cost of the pronounced distortion in $AlP_{Nap}$. Further structural insights can be drawn from the optimized geometries of the adducts AD-$AlP_{Nap}$ and AD-$AlP_{Bph}$, shown in Fig. S2. AD-$AlP_{Nap}$ appears to be more distorted than AD-$AlP_{Bph}$. The NBO analysis reveals strong orbital charge transfer (OCT) from the σ(Al–H2) bonding orbital to the σ*(P–H1) antibonding orbital, with stabilization energies of 57.4 kcal $mol^{-1}$ for $AlP_{Nap}$ and 51.4 kcal $mol^{-1}$ for $AlP_{Bph}$. These strong OCT interactions indicate significant electronic perturbation and rationalize the observed instability of both adducts. Similar, observation can also be made for the $BP_{Nap}$ and $B_{Bph}$ form the Fig. S3 and S4 in the SI.

Among all the IFLPs investigated in this study, the geminally bridged IFLPs represent a particularly interesting case. The optimized structure of $AlP_{Gem}$, along with the key natural bond orbitals (NBOs), is shown in Fig. 5a. The corresponding transition state (TS-$AlP_{Gem}$) and adduct (AD-$AlP_{Gem}$) geometries, including relevant bond lengths and angles, are provided in Fig. 5b and c, respectively. Additionally, the optimized geometries and NBO plots for the boron analogue ($BP_{Gem}$), including TS-$BP_{Gem}$ and AD-$BP_{Gem}$, are presented in Fig. S5 of the SI. As illustrated in Fig. 5a, the optimized geometry of $AlP_{Gem}$ shows an Al–P distance of 3.28 Å, with the Al and P centres oriented away from each other, in contrast to the close proximity observed in other AlP-based IFLPs. NBO analysis reveals the presence of a lone pair orbital on phosphorus (lp(P)) and an empty p orbital on aluminum (p(Al)), both aligned parallel to one another but perpendicular to the molecular plane. Notably, no orbital charge transfer (OCT) from lp(P) to p(Al) is observed. Instead, two distinct charge transfer interactions are present: π(C1═C2) → p(Al) and lp(P) → π*(C1═C2), with stabilization energies of 7.81 kcal $mol^{-1}$ and 6.10 kcal $mol^{-1}$, respectively (see Fig. 5a). These interactions are likely responsible for the unique structural arrangement of $AlP_{Gem}$. The parallel orientation of the electron-rich lp(P) and electron-deficient p(Al) orbitals provides spatially separated reactive sites, allowing for synergistic activation of the $H_2$ molecule. This structural feature plays a critical role in the reactivity of $AlP_{Gem}$.

In the transition state (TS-$AlP_{Gem}$), the Al–P distance shortens to 3.09 Å, and the key geometrical parameters associated with $H_2$ activation—namely the H1–H2, P–H1, and Al–H2 bond lengths are 1.15 Å, 1.60 Å, and 1.77 Å, respectively. The dihedral angle ∠H1–P–Al–H2 is calculated to be −3.9°. The total strain energy in TS-$AlP_{Gem}$ is 54.49 kcal $mol^{-1}$, the lowest among all the transition states investigated in this study. This relatively low strain correlates with the lower relative energy of TS-$AlP_{Gem}$. In the resulting adduct (AD-$AlP_{Gem}$), the structural parameters of the TS-$AlP_{Gem}$ changes to 2.70 Å (H1–H2), 1.39 Å (P–H1), 1.64 Å (Al–H1), and −31.6°(∠H1–P–Al–H2). The increased H1–H2 bond length and the substantial change in dihedral angle suggest that the Al–H2 and P–H1 bonds are spatially oriented away from each other, thereby minimizing intramolecular interaction. This spatial separation likely contributes to the enhanced stability of the adduct, as reflected in both its optimized geometry and electronic structure. A similar behaviour is observed in $BP_{Gem}$, which also features parallel lp(P) and p(B) orbitals. These arise from π(C1═C2) → p(B) and lp(P) → π*(C1═C2) orbital charge transfers, with associated stabilization energies of 21.11 kcal $mol^{-1}$ and 4.85 kcal $mol^{-1}$, respectively (see Fig. S5). The greater stabilization from π(C1═C2) → p(B) charge transfer effectively occupies the p(B) orbital, reducing its availability for interaction with $H_2$. As a result, $BP_{Gem}$ exhibits a higher $H_2$ activation barrier, as evident from Fig. 2. This reduced reactivity is also reflected in the interaction energy between $H_2$ and $BP_{Gem}$ in the transition state. The calculated interaction energy in TS-$BP_{Gem}$ is −28.74 kcal $mol^{-1}$, which is less favourable compared to −33.03 kcal $mol^{-1}$ in TS-$AlP_{Gem}$. Consequently, $BP_{Gem}$ displays a higher $\Delta G$ for the transition state than $AlP_{Gem}$. Further, the geometrical parameters obtained from the optimized structure of AD-$BP_{Gem}$ (Fig. S6) support the observed order of Gibbs free energies ($\Delta G$) of the adducts, consistent with the trends seen in AD-$AlP_{Gem}$. The structural features of AD-$BP_{Gem}$ reflect reduced stabilization compared to AD-$AlP_{Gem}$, thereby explaining its relatively higher $\Delta G$ and lower thermodynamic stability.

Having examined each linker system individually, it is instructive to consolidate these findings and establish the underlying reasons for the divergent behavior of Al–P and B–P IFLPs.

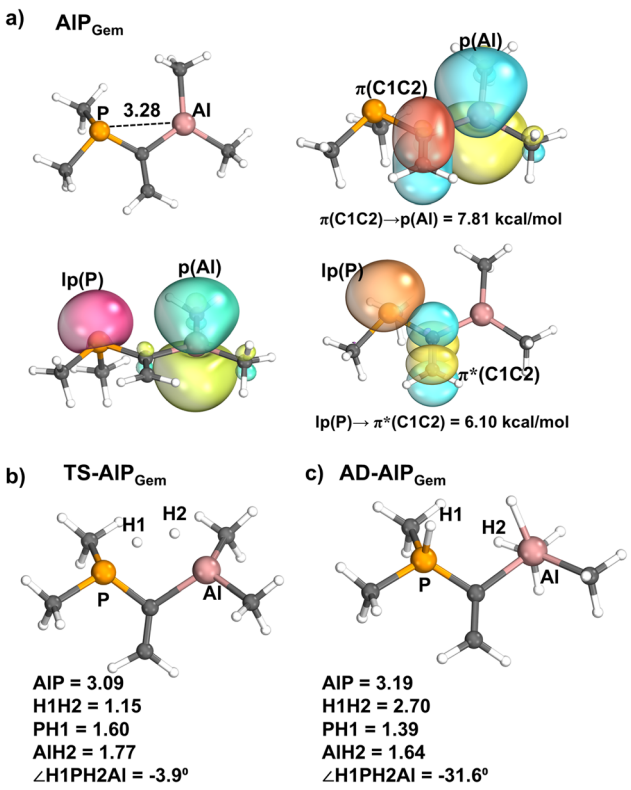


Fig. 5 (a) Optimized geometry of the $AlP_{Gem}$ and NBO plots indicating important orbitals and OCTs, optimized geometry of (b) of TS-$AlP_{Gem}$ and (c) AD-$AlP_{Gem}$ along with important geometrical parameters. (All the distances are in Å).

## Discussion

A broader perspective can be drawn by integrating the observations across all linker types and directly contrasting the AlP and BP systems. The unifying conclusion from the structure analysis is that AlP IFLPs frequently exhibit masked behavior due to partial AlP bonding, while BP analogues consistently retain classical frustrated Lewis pair character. In AlP systems such as $AlP_{Eth}$, $AlP_{Vic}$, $AlP_{Nap}$, and $AlP_{Bph}$, the presence of a BCP and a σ(Al–P) orbital, as revealed by QTAIM and NBO analysis, confirms a tangible AlP bonding interaction. This interaction stabilizes the parent structures but reduces the extent of open frustration, necessitating AlP bond elongation during $H_2$ activation. In contrast, for BP analogues, $BP_{Eth}$ and $BP_{Vic}$, no B–P bond was identified; instead, a donor–acceptor interaction between lp(P) and p(B) has been observed. This fundamental difference underscores the susceptibility of AlP systems towards strain and bond reorganization, while BP IFLPs remain dictated by the accessibility of the empty boron orbital and the geometric proximity enforced by the linker. The ethyl- and vinyl-bridged cases clearly illustrate this point. $AlP_{Eth}$ and $AlP_{Vic}$ exhibit similar activation barriers, despite differences in flexibility, because both must elongate a pre-existing Al–P bond during reaction. Their masked nature is reflected in comparable electronic structures and strain–interaction balances. On the other hand, $BP_{Eth}$ and $BP_{Vic}$ behave differently, $BP_{Eth}$ has a higher barrier, while $BP_{Vic}$ shows an approximately 4 kcal $mol^{-1}$ reduction, attributable to improved orbital overlap between lp(P) and p(B) in the more rigid framework. This divergent response to the same modification highlights the contrasting mechanistic origins of frustration. For AlP, masking by bond formation dominates and is only weakly influenced by ethyl *versus* vinyl flexibility, whereas for BP, the absence of bond masking makes the system more responsive to linker imposed preorganization.

The rigid aromatic linkers provide another interesting comparison. In $AlP_{Nap}$, the shortest Al–P bond distance (2.49 Å) among all AlP systems intensifies the masked character, resulting in the largest strain energy of 80.87 kcal $mol^{-1}$ at the transition state. This strain penalty translates directly into the highest energy barrier for $H_2$ activation. Conversely, $AlP_{Bph}$, though also strained, begins from a more bent geometry with an Al–P bond of 2.75 Å and requires less distortion, leading to a lower barrier. The BP analogues follow the same trend of $BP_{Nap}$ being less favorable than $BP_{Bph}$, but the origin differs. For $BP_{Nap}$ and $BP_{Bph}$, the key factor is not the breaking of a B–P bond, since none exists, but rather the geometric rigidity imposed by the aromatic backbone and its effect on aligning lp(P) and p(B). Thus, while both Al–P and B–P systems show reduced reactivity in naphthyl-linked cases, AlP systems are penalized by bond elongation and excessive distortion, whereas BP systems are destabilized by restricted flexibility and electronic delocalization.

The geminally bridged systems further emphasize the contrast. $AlP_{Gem}$ emerges as the most reactive AlP system, with the lowest transition state energy (29.6 kcal $mol^{-1}$) and the most stable adduct (13.6 kcal $mol^{-1}$). This favorable profile arises because the geminal bridge prevents effective overlap between lp(P) and p(Al), thereby suppressing masking and preserving true frustration. NBO analysis confirms the absence of lp(P) → p(Al) charge transfer, with stabilization instead arising from π(C=C) → p(Al) and lp(P) → π*(C=C) interactions. This arrangement aligns the reactive orbitals in parallel, providing spatially separated acid and base sites that synergistically activate $H_2$. In contrast, the BP analogue $BP_{Gem}$ exhibits a much higher barrier (38.4 kcal $mol^{-1}$). The p(B) orbital is significantly stabilized by π(C=C) → p(B) charge transfer, reducing its availability to accept electron density during $H_2$ activation. As a result, $BP_{Gem}$ shows weaker interaction energies with $H_2$ and a less stable adduct. The geminal case thus demonstrates how identical bridging units can optimize AlP systems by unmasking reactivity but hinder B–P systems by saturating the boron acceptor orbital.

Together, these comparisons establish that the same structural motif can exert fundamentally different effects depending on the nature of the Lewis acidic center. In AlP IFLPs, the masked character requires careful management of AlP interactions that is flexible linkers like ethyl or geminal arrangements reduce masking and yield lower barriers, while overly rigid linkers like naphthyl exacerbate distortion and raise barriers. In BP systems, the absence of masking means that linker effects are transmitted directly to orbital alignment and charge transfer, making rigid frameworks such as vinyl or biphenylene beneficial while naphthyl introduces excessive destabilization. Thus, linker flexibility stabilizes AlP systems but has limited impact on BP, whereas rigid preorganization is advantageous for BP but energetically costly for AlP. These findings complement prior literature that studied either AlP or BP systems in isolation.

From a design perspective, these results imply that AlP systems benefit from strategies that minimize AlP overlap, such as geminal bridges or flexible tethers, while BP systems are more effectively tuned through rigid linkers that promote orbital alignment without excessive strain. This distinction provides a rational basis for tailoring intramolecular FLPs toward specific applications. By identifying the contrasting roles of strain and orbital interactions in AlP *versus* BP systems, the present comparative framework extends beyond $H_2$ activation and can guide the design of element-specific FLPs for activation of other small molecules such as $CO_2$, olefins, and C–H or C–F bonds.

## Conclusion

In this study, the activation of dihydrogen was employed as a diagnostic tool to assess and compare the degree of frustration in a series of structurally analogous AlP- and BP-based intramolecular frustrated Lewis pairs (IFLPs). Through detailed DFT investigations, the impact of various bridging units ranging from flexible (ethyl, vinyl) to rigid (naphthyl, biphenylene, geminal), on the geometric distortion, orbital interactions, and energetic profiles was systematically analyzed. The calculated Gibbs free energies for transition states and

adducts served as key metrics for quantifying the degree of frustration within each system. A fundamental difference in the electronic nature of Al–P and B–P pairs emerged. AlP-IFLPs generally exhibit masked character due to partial Al–P bonding, while BP-IFLPs behave as classical, unmasked FLPs with spatially separated acid–base centres. Despite structural similarities, these intrinsic differences led to distinct responses upon modification of the bridging unit. For example, the geminal-bridged $AlP_{Gem}$ displayed the lowest transition-state energy, highlighting its optimal balance between structural preorganization and electronic separation. Conversely, systems like $AlP_{Nap}$, though preorganized, exhibited high strain penalties upon activation, leading to reduced reactivity. This comparative approach establishes $H_2$ activation not as an end goal, but as a measure of structural and electronic frustration in FLPs. The insights derived here provide a foundational framework for rational FLP design, emphasizing the importance of tuning not only the acid–base strength but also the spatial and electronic interplay enforced by the linker. Future work may extend this methodology to predict and tailor reactivity toward more challenging small molecules.

## Conflicts of interest

The authors declare no competing financial interests.

## Data availability

The data supports the findings is provided in the manuscript and the SI. Supplementary information: images of the optimized structure, NBO plots are given. The coordinates of the optimized structures are also provided. See DOI: **https://doi.org/10.1039/d5ra05892a**.

## Acknowledgements

This work is supported by SERB (EEQ/2023/000424, EEQ/2019/000656 and ECR/2018/002346). With due respect and sense of obligation we would like to thank NIT Warangal for providing necessary facilities during the research work. The authors M. F. is thankful to the Ministry of Education (MoE), formerly the Ministry of Human Resource Development (MHRD) for providing Senior Research Fellowship (SRF).

## References

1 G. C. Welch, R. R. S. Juan, J. D. Masuda and D. W. Stephan, Reversible, Metal-Free Hydrogen Activation, *Science*, 2006, **314**, 1124–1126.
2 D. W. Stephan and G. Erker, Frustrated Lewis pair chemistry of carbon, nitrogen and sulfur oxides, *Chem. Sci.*, 2014, **5**, 2625–2641.
3 D. W. Stephan, Frustrated Lewis Pairs: From Concept to Catalysis, *Acc. Chem. Res.*, 2015, **48**, 306–316.
4 D. W. Stephan, Frustrated Lewis Pairs, *J. Am. Chem. Soc.*, 2015, **137**, 10018–10032.
5 D. W. Stephan and G. Erker, Frustrated Lewis Pair Chemistry: Development and Perspectives, *Angew. Chem., Int. Ed.*, 2015, **54**, 6400–6441.
6 S. A. Weicker and D. W. Stephan, Main Group Lewis Acids in Frustrated Lewis Pair Chemistry: Beyond Electrophilic Boranes, *Bull. Chem. Soc. Jpn.*, 2015, **88**, 1003–1016.
7 D. W. Stephan, The broadening reach of frustrated Lewis pair chemistry, *Science*, 2016, **354**(6317), 1248.
8 A. R. Jupp and D. W. Stephan, New Directions for Frustrated Lewis Pair Chemistry, *Trends Chem.*, 2019, **1**, 35–48.
9 J. Lam, K. M. Szkop, E. Mosaferi and D. W. Stephan, FLP catalysis: main group hydrogenations of organic unsaturated substrates, *Chem. Soc. Rev.*, 2019, **48**, 3592–3612.
10 J. Paradies, Mechanisms in Frustrated Lewis Pair-Catalyzed Reactions, *Eur. J. Org Chem.*, 2019, **2019**, 283–294.
11 N. Li and W. Zhang, Frustrated Lewis Pairs: Discovery and Overviews in Catalysis, *Chin. J. Chem.*, 2020, **38**, 1360–1370.
12 D. W. Stephan, Diverse Uses of the Reaction of Frustrated Lewis Pair (FLP) with Hydrogen, *J. Am. Chem. Soc.*, 2021, **143**, 20002–20014.
13 M. Ghara, H. Mondal, R. Pal and P. K. Chattaraj, Frustrated Lewis Pairs: Bonding, Reactivity, and Applications, *J. Phys. Chem. A*, 2023, **127**, 4561–4582.
14 F.-G. Fontaine and D. W. Stephan, On the concept of frustrated Lewis pairs, *Philos. Trans. R. Soc., A*, 2017, **375**, 20170004.
15 J. S. J. McCahill, G. C. Welch and D. W. Stephan, Reactivity of "Frustrated Lewis Pairs": Three-Component Reactions of Phosphines, a Borane, and Olefins, *Angew. Chem., Int. Ed.*, 2007, **46**, 4968–4971.
16 M. A. Dureen and D. W. Stephan, Terminal Alkyne Activation by Frustrated and Classical Lewis Acid/Phosphine Pairs, *J. Am. Chem. Soc.*, 2009, **131**, 8396–8397.
17 M.-A. Légaré, M.-A. Courtemanche, É. Rochette and F.-G. Fontaine, Metal-free catalytic C–H bond activation and borylation of heteroarenes, *Science*, 2015, **349**, 513–516.
18 K. Lye and R. D. Young, A review of frustrated Lewis pair enabled monoselective C–F bond activation, *Chem. Sci.*, 2024, **15**, 2712–2724.
19 M. Hong, J. Chen and E. Y.-X. Chen, Polymerization of Polar Monomers Mediated by Main-Group Lewis Acid–Base Pairs, *Chem. Rev.*, 2018, **118**, 10551–10616.
20 R. C. Neu, E. Y. Ouyang, S. J. Geier, X. Zhao, A. Ramos and D. W. Stephan, Probing substituent effects on the activation of $H_2$ by phosphorus and boron frustrated Lewis pairs, *Dalton Trans.*, 2010, **39**, 4285.
21 J. J. Cabrera-Trujillo and I. Fernández, Aromaticity can enhance the reactivity of P-donor/borole frustrated Lewis pairs, *Chem. Commun.*, 2019, **55**, 675–678.
22 J. J. Cabrera-Trujillo and I. Fernández, Aromaticity-enhanced reactivity of geminal frustrated Lewis pairs, *Chem. Commun.*, 2022, **58**, 6801–6804.
23 Y. Li and J. Zhu, Achieving a Favorable Activation of the C–F Bond over the C–H Bond in Five- and Six-Membered Ring Complexes by a Coordination and Aromaticity Dually Driven Strategy, *Organometallics*, 2021, **40**, 3397–3407.

24 D. Zhuang, Y. Li and J. Zhu, Antiaromaticity-Promoted Activation of Dihydrogen with Borole Fused Cyclooctatetraene Frustrated Lewis Pairs: A Density Functional Theory Study, *Organometallics*, 2020, **39**, 2636–2641.

25 D. Zhuang, A. M. Rouf, Y. Li, C. Dai and J. Zhu, Aromaticity-promoted $CO_2$ Capture by P/N-Based Frustrated Lewis Pairs: A Theoretical Study, *Chem.–Asian J.*, 2020, **15**, 266–272.

26 M. Faizan, A. Kumar, M. Raghasudha and R. Pawar, PIO and IBO analysis to unravel the hidden details of the $CO_2$ sequestration mechanism of aromatically tempered N/B-based IFLPs, *Phys. Chem. Chem. Phys.*, 2023, **25**, 24809–24818.

27 M. Faizan, M. Chakraborty, D. Bana and R. Pawar, Orbital and free energy landscape expedition towards the unexplored catalytic realm of aromatically modified FLPs for $CO_2$ sequestration, *Phys. Chem. Chem. Phys.*, 2024, **26**, 23609–23622.

28 M. Faizan, S. Yadav and R. Pawar, Aromatic Tempering Unlocks the Unseen Bonding Behavior of Phosphorus/Boron FLPs at the Trade of Reactivity, *Inorg. Chem.*, 2025, **64**, 10724–10728.

29 F. Krämer, Aluminum in Frustrated Lewis Pair Chemistry, *Angew. Chem., Int. Ed.*, 2024, **63**, e202405207.

30 T. Kaehler and R. L. Melen, Comparative study of fluorinated triarylalanes and their borane counterparts, *Cell Rep. Phys. Sci.*, 2021, **2**(10), 100595.

31 G. Ménard and D. W. Stephan, C≡H Activation of Isobutylene Using Frustrated Lewis Pairs: Aluminum and Boron σ-Allyl Complexes, *Angew. Chem., Int. Ed.*, 2012, **51**, 4409–4412.

32 G. Ménard, L. Tran, J. S. J. McCahill, A. J. Lough and D. W. Stephan, Contrasting the Reactivity of Ethylene and Propylene with P/Al and P/B Frustrated Lewis Pairs, *Organometallics*, 2013, **32**, 6759–6763.

33 G. Ménard and D. W. Stephan, Stoichiometric Reduction of $CO_2$ to CO by Aluminum-Based Frustrated Lewis Pairs, *Angew. Chem., Int. Ed.*, 2011, **50**, 8396–8399.

34 G. Ménard and D. W. Stephan, $H_2$ Activation and Hydride Transfer to Olefins by $Al(C_6F_5)_3$-Based Frustrated Lewis Pairs, *Angew. Chem., Int. Ed.*, 2012, **51**, 8272–8275.

35 F. Krämer, J. Paradies, I. Fernández and F. Breher, Quo Vadis $CO_2$ Activation: Catalytic Reduction of $CO_2$ to Methanol Using Aluminum and Gallium/Carbon-based Ambiphiles, *Chem.–Eur. J.*, 2024, **30**, e202303380.

36 C. Appelt, H. Westenberg, F. Bertini, A. W. Ehlers, J. C. Slootweg, K. Lammertsma and W. Uhl, Geminal Phosphorus/Aluminum-Based Frustrated Lewis Pairs: C≡H *versus* C≡C Activation and $CO_2$ Fixation, *Angew. Chem., Int. Ed.*, 2011, **50**, 3925–3928.

37 D. Pleschka, M. Layh, F. Rogel and W. Uhl, Structure and reactivity of an Al/P-based frustrated Lewis pair bearing relatively small substituents at aluminium, *Philos. Trans. R. Soc., A*, 2017, **375**, 20170011.

38 W. Uhl, J. Backs, A. Hepp, L. Keweloh, M. Layh, D. Pleschka, J. Possart and A. Wollschläger, Reactions of Al/P, Ga/P and P–H functionalized frustrated Lewis pairs with azides and a diazomethane – formation of adducts and capture of nitrenes, *Z. Naturforsch. B*, 2017, **72**, 821–838.

39 P. Federmann, T. Bosse, S. Wolff, B. Cula, C. Herwig and C. Limberg, A strained intramolecular P/Al-FLP and its reactivity toward allene, *Chem. Commun.*, 2022, **58**, 13451–13454.

40 M. E. A. Dilanas and F. Breher, Reactivity of an *Ortho*-Phenylene-Bridged Al/P Frustrated Lewis Pair toward Small Molecules, *Eur. J. Inorg. Chem.*, 2025, **28**, e202500174.

41 S. Portela and I. Fernández, Understanding the enhanced reactivity of strained intramolecular Frustrated Lewis Pairs, *Z. Anorg. Allg. Chem.*, 2023, **649**, e202200384.

42 P. Federmann, R. Müller, F. Beckmann, C. Lau, B. Cula, M. Kaupp and C. Limberg, Synthesis of Intramolecular P/Al-Based Frustrated Lewis Pairs *via* Aluminum-Tin-Exchange and their Reactivity toward $CO_2$, *Chem.–Eur. J.*, 2022, **28**, e202200404.

43 E. G. Hohenstein, S. T. Chill and C. D. Sherrill, Assessment of the Performance of the M05−2X and M06−2X Exchange-Correlation Functionals for Noncovalent Interactions in Biomolecules, *J. Chem. Theory Comput.*, 2008, **4**, 1996–2000.

44 K. B. Wiberg, *Ab Initio* Molecular Orbital Theory by W. J. Hehre, L. Radom, P. V. R. Schleyer, and J. A. Pople, John Wiley, New York, 548pp. Price: $79.95 (1986), *J. Comput. Chem.*, 1986, **7**, 379.

45 W. M. Dagnaw and A. M. Mohammed, Computational Design of Frustrated Lewis Pairs as a Strategy for Catalytic Hydrogen Activation and Hydrogenation Catalyst, *ACS Omega*, 2023, **8**, 8488–8496.

46 P. Sarkar, S. Das and S. K. Pati, Assessing Tetrel-Based Neutral Frustrated Lewis Pairs for Catalytic Hydrogenation, *J. Phys. Chem. C*, 2021, **125**, 22522–22530.

47 Y. Li, C. Hou, J. Jiang, Z. Zhang, C. Zhao, A. J. Page and Z. Ke, General $H_2$ Activation Modes for Lewis Acid–Transition Metal Bifunctional Catalysts, *ACS Catal.*, 2016, **6**, 1655–1662.

48 K. Wang, L. Cheng, J. Zhang and X. Yu, The mechanism of the chain-growth of ammoniaborane: A classic Lewis pairs catalysed by a Frustrated Lewis Pairs, *Int. J. Hydrogen Energy*, 2018, **43**, 4177–4185.

49 P. Sarkar, S. Das and S. K. Pati, Investigating Tetrel-Based Neutral Frustrated Lewis Pairs for Hydrogen Activation, *Inorg. Chem.*, 2021, **60**, 15180–15189.

50 Y. Guo, X. Lian, H. Zhang, X. Zhang, J. Chen, C. Chen, X. Lan and Y. Shao, Systematic Assessment of the Catalytic Reactivity of Frustrated Lewis Pairs in C–H Bond Activation, *Molecules*, 2023, **29**, 24.

51 A. V. Marenich, C. J. Cramer and D. G. Truhlar, Universal Solvation Model Based on Solute Electron Density and on a Continuum Model of the Solvent Defined by the Bulk Dielectric Constant and Atomic Surface Tensions, *J. Phys. Chem. B*, 2009, **113**, 6378–6396.

52 M. J. Frisch, G. W. Trucks, H. B. Schlegel, G. E. Scuseria, M. A. Robb, J. R. Cheeseman, G. Scalmani, V. Barone, G. A. Petersson, H. Nakatsuji, X. Li, M. Caricato, A. V. Marenich, J. Bloino, B. G. Janesko, R. Gomperts, B. Mennucci, H. P. Hratchian, J. V. Ortiz, A. F. Izmaylov,

J. L. Sonnenberg, D. Williams-Young, F. Ding, F. Lipparini, F. Egidi, J. Goings, B. Peng, A. Petrone, T. Henderson, D. Ranasinghe, V. G. Zakrzewski, J. Gao, N. Rega, G. Zheng, W. Liang, M. Hada, M. Ehara, K. Toyota, R. Fukuda, J. Hasegawa, M. Ishida, T. Nakajima, Y. Honda, O. Kitao, H. Nakai, T. Vreven, K. Throssell, J. A. Montgomery Jr, J. E. Peralta, F. Ogliaro, M. J. Bearpark, J. J. Heyd, E. N. Brothers, K. N. Kudin, V. N. Staroverov, T. A. Keith, R. Kobayashi, J. Normand, K. Raghavachari, A. P. Rendell, J. C. Burant, S. S. Iyengar, J. Tomasi, M. Cossi, J. M. Millam, M. Klene, C. Adamo, R. Cammi, J. W. Ochterski, R. L. Martin, K. Morokuma, O. Farkas, J. B. Foresman and D. J. Fox, *Gaussian 16 Rev. C.01* , Wallingford, CT, 2016.

53 E. D. Glendening, C. R. Landis and F. Weinhold, NBO 7.0: New vistas in localized and delocalized chemical bonding theory, *J. Comput. Chem.*, 2019, **40**, 2234–2241.

54 R. F. W. Bader, Atoms in molecules, *Acc. Chem. Res.*, 1985, **18**, 9–15.

55 R. F. W. Bader, *Atoms in Molecules: A Quantum Theory*, Oxford University PressOxford, 1990.

56 *The Quantum Theory of Atoms in Molecules: From Solid State to DNA and Drug Design*, ed. C. F. Matta and R. J. Boyd, Wiley, 1st edn, 2007.

57 T. Lu and F. Chen, Multiwfn: A multifunctional wavefunction analyzer, *J. Comput. Chem.*, 2012, **33**, 580–592.

58 W.-J. Van Zeist and F. M. Bickelhaupt, The activation strain model of chemical reactivity, *Org. Biomol. Chem.*, 2010, **8**, 3118.